Bubble cloud depth under a hurricane

D. W. Wang,[1] H. W. Wijesekera,[1] W. J. Teague,[1] W. E. Rogers,[1] and E. Jarosz[1]

[1]   The bubble cloud depth and its correlation with extreme winds are key elements of bubble-mediated gas injection, which are critical to the determination of the global gas budgets. The characteristics of bubble cloud depth were examined from measurements collected during the passage of a category-4 hurricane with winds up to 50 m s^{-1}. The bubble cloud depth increases linearly with wind speed for winds less than 35 m s^{-1}. Our findings are consistent with previous observations at low to moderate wind speeds. However, the rate of increase is reduced significantly at winds higher than 35 m s^{-1}. **Citation:** Wang, D. W., H. W. Wijesekera, W. J. Teague, W. E. Rogers, and E. Jarosz (2011), Bubble cloud depth under a hurricane, *Geophys. Res. Lett.*, *38*, L14604, doi:10.1029/2011GL047966.

1.   Introduction

[2]   Bubble clouds generated by breaking waves play an important role in gas exchange between the atmosphere and upper-ocean. Formation of bubble clouds during storms is responsible for injecting nitrogen and oxygen gases that can supersaturate the ocean [*Vagle et al.*, 2010]. Field data from Hurricane Frances (2004) indicated that the complete bubble injection process at high winds becomes an important factor in the air-sea gas exchange process [*D'Asaro and McNeil*, 2007; *McNeil and D'Asaro*, 2007]. Recently, oxygen and nitrogen gas injection coefficients are shown to be related to the bubble cloud depth during winter storms over the northwest Pacific Ocean [*Vagle et al.*, 2010]. Observations of bubble cloud depth evolution directly under hurricane paths are extremely rare due to the logistics of making such measurements. As a result, characteristics of bubble cloud depth and their correlations with wind forces are not well understood. These are key elements to the understanding of the injection of weakly soluble gases such as nitrogen and oxygen, which is becoming more critical to the determination of the global gas budgets, and ultimately to the global climate since the number and intensity of storms appears to be increasing over the past and future decades [*Emanuel*, 2005; *Bender et al.*, 2010].

[3]   A unique data set of acoustic backscatter was collected under a category-4 hurricane, Ivan in 2004, on the continental shelf in the northeastern Gulf of Mexico as part of the Naval Research Laboratory's (NRL's) Slope to Shelf Energetics and Exchange Dynamics (SEED) project [*Teague et al.*, 2007]. Hurricane Ivan passed directly over the SEED mooring array on around 0000 UTC, 16 September 2004 (Figure 1) [*Teague et al.*, 2007]. Although the main observations from SEED are

current velocity profiles, the data set also contains profiles of acoustic backscatter from six bottom-mounted acoustic Doppler current profilers (ADCPs) near 29.4°N, 88°W. This study examines acoustic backscattering intensity as a measure of bubble concentration along the path of Hurricane Ivan. The main objective of this study is to quantify the bubble cloud depths and their relationships to wind speed.

2.   Measurements and Analysis

[4]   During NRL's SEED project, six Barny moorings were deployed on the outer continental shelf along 60-m and 90-m isobaths. M1, M2, and M3 were on the 60-m isobath and M4, M5, and M6 were on the 90-m isobath (Figure 1). Moorings were spaced approximately 15 km apart on each isobaths. Each mooring carried a 300-kHz RD Instruments Workhorse ADCP and a wave/tide gauge. ADCPs rested about 0.5 m above the ocean floor with four transducers, each with an incidence angle of 20 degrees. Echo intensity profiles with 2-m cell resolution were ensemble averages of 55 pings that were transmitted over a 15-min period for each transducer beam. The depth reference for ADCP profiles was taken as the distance from the mean sea surface, which was estimated from the 15-minute averaged bottom pressure with a correction of sea surface pressure [*Wang et al.*, 2005]. The echo intensity was converted to volumetric backscatter strength M_v in m^{-1} by the use of the sonar equation with calibration coefficients provided by the manufacturer, Teledyne RD Instruments (http://www.rdinstruments.com/). Details of the backscatter equation and coefficients are given by *Deines* [1999]. The backscattering strength is also expressed as $S_v = 10 \log_{10}(M_v)$, where S_v is in dB. The backscattering data from the near-surface ADCP-cells were likely contaminated by the side-lobe effect, and therefore we excluded data from the 3.6-m and 5.4-m cell depths for the 60-m and 90-m deployments, respectively. The cells near the mean sea level would be above or below of the ocean wave surface during data acquisition. In this study, we excluded backscattering data from the cells that were within the amplitude of the surface waves relative to the mean sea level. Here, the wave amplitude was taken as the half of significant wave height ($H_s/2$). In addition, the averaged ADCP backscatter profiles were based on a depth reference with respect to mean sea level, which led to a larger backscatter S_v than those based on a depth reference with respect to the wave surface [*Thorpe*, 1982].

[5]   Backscatter profiles for each SEED mooring were constructed by averaging of the profiles of four transducer beams. The averaged profile of acoustic backscatter M_v shows an exponential decrease with depth, and can be expressed as $M_v = M_0 \exp(-z/L)$, where z is the depth below mean sea level; M_0 is the backscatter level at z = 0; and L is the characteristic ("e-folding") length scale, which determines the rate of decrease of M_v with increasing depth [*Thorpe*,

[1]Naval Research Laboratory, Stennis Space Center, Mississippi, USA.
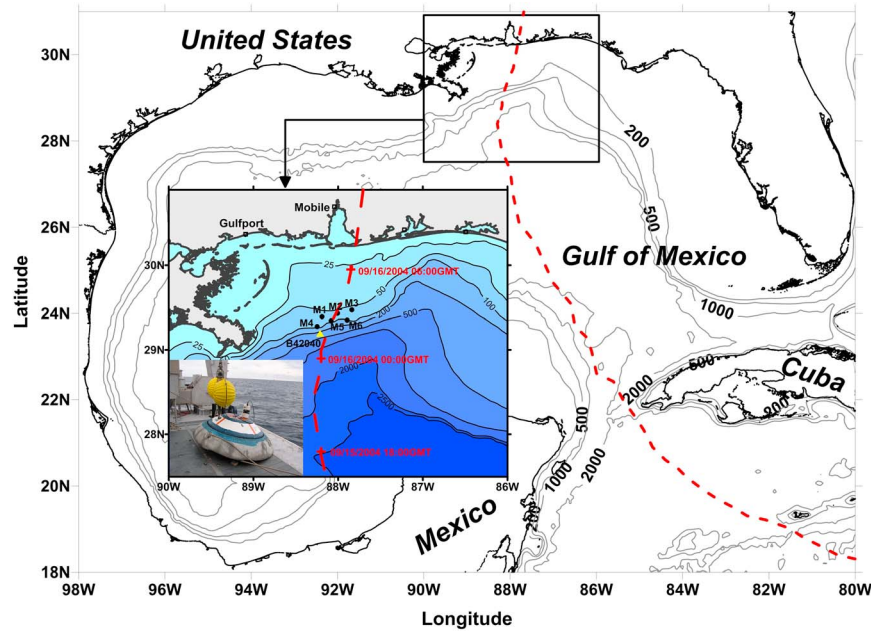
Figure 1. Path of Hurricane Ivan (red dashed line). Mooring locations at 60 m and 90 m isobaths are marked in solid circles (M1–M6). The yellow triangle is the NDBC buoy 42040. The insert shows a BARNY mooring before deployment (lower left). Contour depths are in meters.

1982, 1984; *Trevorrow*, 2003; *Vagle et al.*, 2010]. The entrainment depth of bubbles can be estimated from a given backscatter profile by knowing the noise level of the measurement. Here the bubble cloud depth Z_b was determined to represent the lower boundary of the bubble layer, where the backscatter intensity exceeds an empirically-determined noise threshold M_T. In this study, $M_T = 10^{-6}$ (or $S_v = -60$ dB) which was the noise threshold prior to the arrival of Ivan. Similar techniques have been used to determine bubble cloud depths with slightly different threshold levels, −50dB [*Trevorrow*, 2003] and −70dB [*Vagle et al.*, 2010]. The e-folding length scale, L was estimated by fitting the exponential profile between Z_b and the acceptable shallowest depth.

[6] Ivan approached the mooring site as a category-4 hurricane with a steady speed, direction, and intensity. Its eye passed through the array and hence its extreme winds were prevalent over all six moorings [*Teague et al.*, 2007]. The diameter of the eye was about 50 km. The center of the eye passed directly over the M2 and M5 moorings, while M3 and M6 were located slightly to the right side of the hurricane, and M1 and M4 were located slightly to the left side of the hurricane (Figure 1). Ivan produced extreme waves with significant wave heights higher than 15 m [*Wang et al.*, 2005] and currents of about 2 m s^{-1} [*Teague et al.*, 2007; *Wijesekera et al.* 2010]. During the passage of Ivan on September 16, 2004, the water above each SEED mooring (Figure 1) was well mixed according to the small water temperature difference (<2°C) between the bottom temperature from Barnys and the sea surface temperature from satellite and National Data Buoy Center (NDBC) buoy 42040 [e.g., *Teague et al.*, 2007]. The surface wind over the mooring site was reconstructed by combining wind data from the NDBC buoy 42040 and model winds from the post-storm wind analysis by the Hurricane Research Center (HRD) [*Powell et al.*, 1998; *Wang et al.*, 2005; *Ardhuin et al.*, 2010]. Wave fields at different

mooring locations were obtained from the wave model "WaveWatch III" [*Ardhuin et al.*, 2010] based on HRD winds and NDBC wave buoy data.

[7] As seen in Figure 2a, the hurricane passage over M5 can be divided into four stages. They are: (I) the arrival of the eye-wall with increasing wind, (II) the arrival of the eye with decreasing wind, (III) the departure of the eye with increasing wind until the arrival of backside of eye-wall, and (IV) the departure of the eye-wall with decreasing wind. Hurricane Ivan's eye took about four hours to cross the mooring array. Wind speeds decelerated from 45 m s^{-1} to 15 m s^{-1} and then accelerated back to about 40 m s^{-1}. The backscatter observations from all six moorings were from Ivan's front-right and rear-left quadrants. Figure 2b shows relative locations of M5 to the eye of hurricane and the forward direction.

[8] A dramatic change in the ADCP backscattering strength was found during the passage of Ivan. As shown in Figure 2a, prior to the arrival of Ivan, intense backscatter induced by bubble clouds was limited to about 10 m beneath the mean sea surface. The bubble cloud depth increased with increasing wind speed and wave height. As a result, a backscatter intensity of about −70dB can be found as deep as 40 m when Ivan's eye-wall reached M5 with peak winds of about 45 m s^{-1}. The bubble-induced backscatter layer decreased and increased rapidly when the eye crossed M5 (stages II and III), during which the ocean was experiencing a rapid decrease and increase of winds, surface waves, and near-surface currents. The bubble cloud layer increased rapidly as the eye-wall of Ivan crossed the mooring site for the second time. Similar relationships between the layer of high backscatter intensity and local winds were observed at the rest of the mooring sites. Three selected ADCP backscatter profiles from M5 at wind speeds of 19.9 m s^{-1}, 29.6 m s^{-1} and 41 m s^{-1} are shown in Figure 2c. The bubble cloud depth Z_b is determined as the depth at which $S_v = -60$dB. The backscatter strength between the shallowest uncontaminated depth and
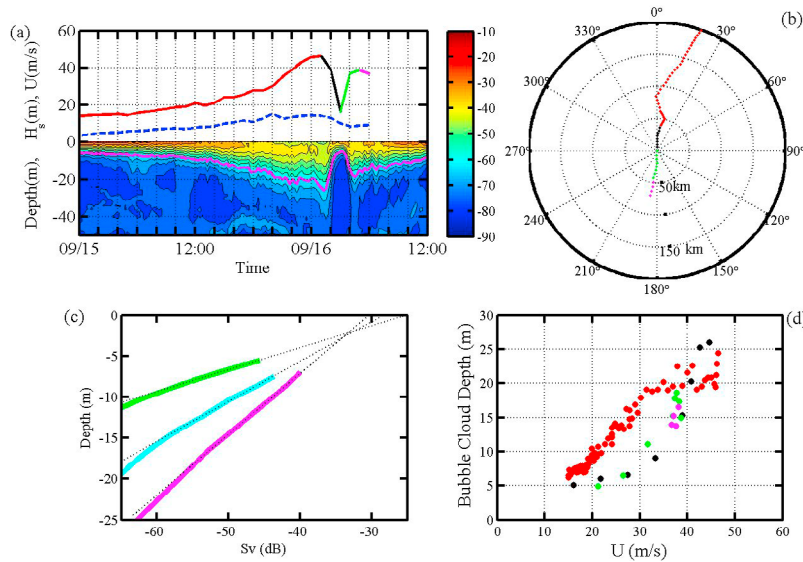
Figure 2. (a) (top) Surface wind at 10 m height (multi- colored solid line) and significant wave height H_s (blue dashed line) at M5 during Ivan's passage. Red, black, green, and magenta wind segments represent the four stages of Ivan's passage, respectively. (bottom) Contour plot of ADCP backscatter profile from M5 during Ivan's passage. −60dB contour line is highlighted as magenta line. (b) Polar plot shows the relative location of M5 with respect to the Ivan's center and its forward propagation direction (0 degree) at the times of backscatter data acquired within 200 km of Ivan center (after 1630 UTC 15 September). Radial distance is in km. Color symbols represent the four stages as defined in Figure 2a. (c) Three ADCP backscatter depth profiles from M5 at 12:45 UTC (green), 19:45 UTC (cyan), and 22:30 UTC (magenta), September 15 are selected. Winds are 19.9 m s^{-1}, 29.6 m s^{-1} and 41 m s^{-1}, and significant wave heights are 8.1 m, 14.6 m and 13.8 m, respectively. The near-surface sections which were disregarded in the computation are not shown. Black dotted line represents the fitted exponential decrease with depth $M_v = M_0 \exp(-z/L)$ for each profile. (d) Bubble cloud depth Z_b vs. wind speed for the four stages of Ivan's passage from M5. The color symbols represent the four stages as defined in Figure 2a.

Z_b decays exponentially with depth and is well represented by $M_v = M_0 \exp(-z/L)$.

[9] The scatter plot of Z_b versus wind is shown in Figure 2d. For winds less than 15 m s^{-1}, Z_b is relatively independent of wind due to the combined effects of a coarse vertical cell size (2 m) and the side-lobe effect (5.4 m) of the ADCP. Therefore, we focus our analyses for winds larger than 15 m s^{-1}. During the arrival of the eye-wall (stage I), Z_b increased with increasing wind speed. During stages II and III, the bubble cloud depth first decreased and then increased as a result of the dramatic variation of wind speeds across the eye. The bubble cloud depth is closely related to the winds, but the rate of change in bubble cloud depth was generally faster inside the eye-wall than the eye-wall arrival stage (stage I). The differences in the correlation of Z_b with winds at the four hurricane passage stages could be due to variations of breaking-wave characteristics. The averaged relationship between Z_b and wind speed during the growing stage (i.e., stage I, Figure 2d) of the hurricane was examined by averaging Z_b into wind speed bins using data from all six moorings. The bin-averaged bubble depth $\langle Z_b \rangle$ versus wind speed is shown in Figure 3a. $\langle Z_b \rangle$ is closely related to wind speed and increased from about 7.5 m to about 21 m as wind speed increased from 15 m s^{-1} to 35 m s^{-1}. The observed relationship is consistent with results from *Vagle et al.* [2010] based on backscatter profiles observed for winds less than 25 m s^{-1} (dashed blue line in Figure 3a). For winds higher than 35 m s^{-1}, the rate of change of $\langle Z_b \rangle$ became smaller in spite of increasing winds. This coincides with the reduction of
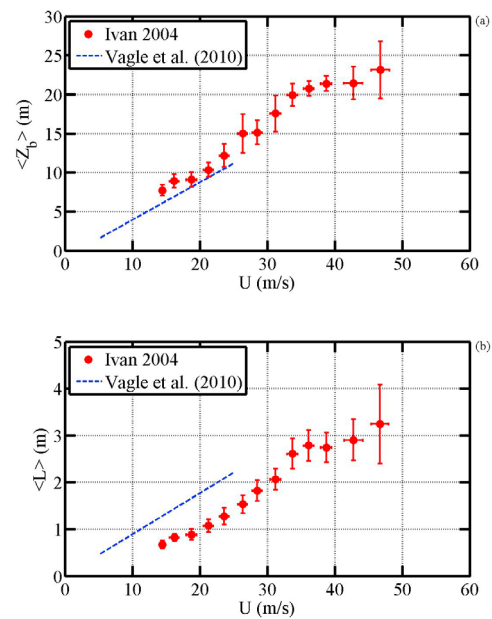
Figure 3. Bin-averaged (a) bubble cloud depth $\langle Z_b \rangle$ and (b) e-folding length $\langle L \rangle$ versus wind speed. Error bar lines indicate one standard deviation. The thick dash lines in Figures 3a and 3b represent the linear relationship from *Vagle et al.* [2010].

the surface drag coefficient at high winds as reported by *Powell et al.* [2003] and *Jarosz et al.* [2007].

[10] The e-folding length L computed from the backscatter profile reflects the rate of the decrease in bubble concentration with an increasing depth. The e-folding length appears to be related to the characteristic length scale associated with the turbulent diffusion coefficient in the surface layer [*Thorpe*, 1984]. As shown in Figure 3b, the bin-averaged e-folding length $\langle L \rangle$ increased from about 0.8 m at winds of 15 m s^{-1} to about 2.8 m at winds of 35 m s^{-1}. The observed growth rate of $\langle L \rangle$ is qualitatively consistent with the linear relation from *Vagle et al.* [2010] based on their measurements for winds under 25 m s^{-1}. Similar to $\langle Z_b \rangle$, $\langle L \rangle$ flattened for winds higher than 35 m s^{-1}. Estimated e-folding lengths from *Vagle et al.* [2010] are higher than our estimates by a factor of 1.5–2. These differences could be because the backscatter profiles from *Vagle et al.* [2010] were based on a depth reference with respect to the wave surface, which can result in a higher e-folding length scale than a depth reference based on a mean sea level as used here [e.g., *Thorpe*, 1982].

3. Discussion and Summary

[11] We examined and quantified the evolution of bubble cloud depth based on measurements during the passage of a category-4 hurricane with winds up to 50 m s^{-1}. We found that the bubble cloud depth and e-folding length scale increase with wind speed. However the growth rates of $\langle Z_b \rangle$ and $\langle L \rangle$ were much reduced when winds exceeded 35 m s^{-1}. The flattening of $\langle Z_b \rangle$ at winds higher than 35 m s^{-1} may explain why gas injection flux peaked at winds of about 37 m s^{-1} during observations of gas transfer rates by *D'Asaro and McNeil* [2007] from Hurricane Frances. These findings on the wind speed-dependent $\langle Z_b \rangle$ and $\langle L \rangle$ lead us to postulate: (a) wind driven turbulences increase Z_b, (b) at high winds, Z_b and L are related to surface drag and (c) the reduced rate of bubble cloud depth and e-folding length at high winds could be due to the combination of the reduction of surface drag [*Jarosz et al.*, 2007; *Powell et al.*, 2003] and the complete bubble dissolving under hydrostatic pressure [*D'Asaro and McNeil*, 2007; *McNeil and D'Asaro*, 2007]. This also implies that the parameterization of air-sea gas exchange based on wind speed alone should be limited to winds up to about 35 m s^{-1}. Extending the wind-speed dependent relation of gas exchange to high winds could result into an overestimation. The dynamics of air-sea momentum transport (such as the complexity of wind-stress dependence on the surface drag coefficient) at the sea surface must be considered for parameterization of gas exchange at high winds.

References

Ardhuin, F., et al. (2010), Semiempirical dissipation source functions for ocean waves. Part I: Definition, calibration, and validation, *J. Phys. Oceanogr.*, 40, 1917–1941, doi:10.1175/2010JPO4324.1

Bender, M. A., T. R. Knutson, R. E. Tuleya, J. J. Sirutis, G. A. Vecchi, S. T. Garner, and I. M. Held (2010), Modeled impact of anthropogenic warming on the frequency of intense Atlantic hurricane, *Science*, 327, 454–458, doi:10.1126/science.1180568.

D'Asaro, E., and C. McNeil (2007), Air-sea exchange at extreme wind speeds, *J. Mar. Syst.*, 66, 92–109.

Deines, K. L. (1999), Backscatter estimation using broadband acoustic Doppler current profilers, in *Proceedings of the IEEE Sixth Working Conference on Current Measurement*, pp. 249–253, Inst. Electr. and Electron. Eng., New York.

Emanuel, K. (2005), Increasing destructiveness of tropical cyclones over the past 30 years, *Nature*, 436, 686–688, doi:10.1038/nature03906.

Jarosz, E., D. A. Mitchell, D. W. Wang, and W. J. Teague (2007), Bottom-up determination of air-sea momentum exchange under a major tropical cyclone, *Science*, 315, 1707–1709, doi:10.1126/science.1136466.

McNeil, C., and E. D'Asaro (2007), Parameterization of air-sea gas fluxes at extreme wind speeds, *J. Mar. Syst.*, 66(1–4), 110–121, doi:10.1016/j.jmarsys.2006.05.013.

Powell, M. D., S. H. Houston, L. R. Amat, and N. Morisseau-Leroy (1998), The HRD real-time hurricane wind analysis system, *J. Wind Eng. Ind. Aerodyn.*, 77–78, 53–64, doi:10.1016/S0167-6105(98)00131-7

Powell, M. D., P. J. Vickery, and T. A. Reinhold (2003), Reduced drag coefficient for high wind speeds in tropical cyclones, *Nature*, 422, 279–283, doi:10.1038/nature01481

Teague, W. J., E. Jarosz, D. W. Wang, and D. A. Mitchell (2007), Observed oceanic response over the upper continental slope and outer shelf during Hurricane Ivan, *J. Phys. Oceanogr.*, 37, 2181–2206, doi:10.1175/JPO3115.1.

Thorpe, S. A. (1982), On the clouds of bubbles formed by breaking wind-waves in deep water, and their role in air–sea gas transfer, *Philos. Trans. R. Soc. London, Ser. A*, 304, 155–210, doi:10.1098/rsta.1982.0011.

Thorpe, S. A. (1984), On the determination of $K\nu$ in the near-surface ocean from acoustic measurements of bubbles, *J. Phys. Oceanogr.*, 14, 855–863, doi:10.1175/1520-0485(1984)014<0855:OTDOIT>2.0.CO;2.

Trevorrow, M. V. (2003), Measurements of near surface bubble plumes in the open ocean with implication for high-frequency sonar performance, *J. Acoust. Soc. Am.*, 114(5), 2672–2684, doi:10.1121/1.1621008.

Vagle, S., C. McNeil, and N. Steiner (2010), Upper ocean bubble measurements from the NE Pacific and estimates of their role in air-sea transfer of the weakly soluble gases nitrogen and oxygen, *J. Geophys. Res.*, 115, C12054, doi:10.1029/2009JC005990.

Wang, D. W., D. A. Mitchell, W. J. Teague, E. Jarosz, and M. S. Hulbert (2005), Extreme waves under hurricane Ivan, *Science*, 309, 896, doi:10.1126/science.1112509.

Wijesekera, H. W., D. W. Wang, W. J. Teague, and E. Jarosz (2010), High sea-floor stress induced by extreme hurricane waves, *Geophys. Res. Lett.*, 37, L11604, doi:10.1029/2010GL043124.

E. Jarosz, W. E. Rogers, W. J. Teague, D. W. Wang, and H. W. Wijesekera, Naval Research Laboratory, Bldg. 1009, Stennis Space Center, MS 39529, USA. (dwang@nrlssc.navy.mil)